

Observations and Modeling of Line Asymmetries in Chromospheric Flares

Arkadiusz Berlicki

Astronomical Institute, Wrocław University, Wrocław, Poland

Abstract. For many years various asymmetrical profiles of different spectral lines emitted from solar flares have been frequently observed. These asymmetries or line shifts are caused predominantly by vertical mass motions in flaring layers and they provide a good diagnostics for plasma flows during solar flares. There are many controversial results of observations and theoretical analysis of plasma flows in solar chromospheric flares. The main difficulty is the interpretation of line shifts or asymmetries. For many years, methods based on bisector techniques were used but they give a reliable results only for some specific conditions and in most cases cannot be applied. The most promising approach is to use the non-LTE techniques applied for flaring atmosphere. The calculation of synthetic line profiles is performed with the radiative transfer techniques and the assumed physical conditions correspond to flaring atmosphere. I will present an overview of different observations and interpretations of line asymmetries in chromospheric flares. I will explain what we have learnt about the chromospheric evaporation in the frame of hydrodynamical models as well as reconnection models. A critical review will be done on the classical methods used to derive Doppler-shifts for optically thick chromospheric lines. In particular, details on the new approach for interpreting chromospheric line asymmetries based on the non-LTE techniques will be presented.

1. Introduction

Spectroscopic observations of solar chromospheric flares show that the line profiles emitted by the flaring plasma almost always exhibit asymmetries or shifts. These features are surely due to the chromospheric plasma motion and the resulting Doppler-shifts effects. Interpretation of the shape of line profiles allows us to understand the nature of plasma flows during solar flares. Plasma flows in the chromosphere are important in the analysis of dynamics and energetics of solar flares as well as these phenomena supply matter to the coronal parts of flares in the process of chromospheric evaporation. Understanding of the mechanisms which generate flows is necessary for complete description of solar flares.

Spectral line asymmetries arise only because of the line-of-sight component of plasma velocity which due to the Doppler-shift is responsible for the modification of spectral line profiles. Therefore, for the flares located on the solar disk center we are able to analyze flows oriented perpendicular to the solar surface. For simplicity, the theoretical analysis of line asymmetries often assume that the emitting region is located on the solar disk center and only vertical flows are present.

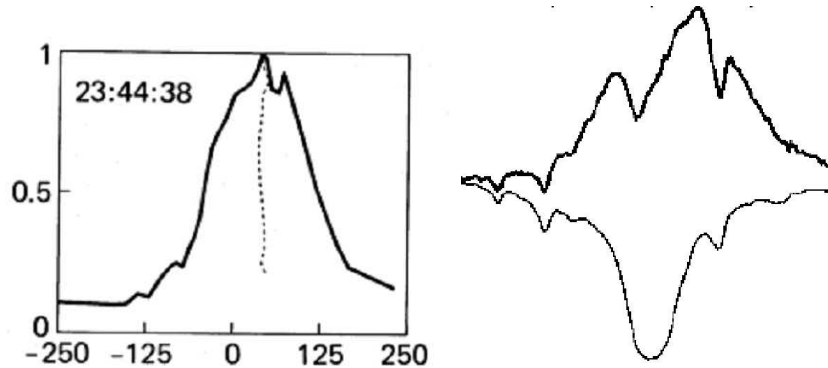


Figure 1. Two examples of the $H\alpha$ line profiles observed during solar flares. *Left*: shifted profile – the Doppler velocity may be determined from the shift of the whole line. *Right*: complicated asymmetric profile – it is impossible to determine the Doppler velocity from such line profile using bisector methods.

Unfortunately, the interpretation of the shape of line profiles is not trivial and to determine the velocity field we must use advanced methods based on hydrodynamical and radiative transfer techniques. There are some rare cases when the interpretation of line asymmetries is relatively simple. When the flow of the whole flaring region is homogeneous then the shape of the line is not disturbed compared to the static symmetric line profile, but the whole line is just shifted towards longer or shorter wavelengths (Fig. 1 – left). We can measure this shift and using a simple Doppler formula calculate specific value of the line-of-sight velocity. Unfortunately, in most cases the line profiles of solar flares exhibit much more complicated structure (Fig. 1 – right) which suggests that the velocity field is not homogeneous and different parts of the flare move in different way.

There are two main approaches to the modeling of chromospheric line asymmetries. One is based on the hydrodynamics calculations, where the time evolution of the solar flare atmosphere is calculated and the radiative transfer formulae are used to calculate the radiation from this evolving atmosphere. Another approach is based on semiempirical models of solar flares.

In this paper I will present a short review on observation and interpretation of the chromospheric line asymmetries observed during solar flares. The term chromospheric lines is commonly used to describe all spectral lines formed in the solar chromosphere, where the temperature is around 10^4 K. These lines are formed in strong non-LTE conditions and complicated radiative transfer calculations are necessary to describe the formation of these lines. Strong chromospheric lines are usually optically thick what means that the optical thickness of the plasma in these lines is very large ($\tau \gg 1$).

There is a wide literature concerning this topic and I provide the readers some references contained the most important results. I will concentrate on chromospheric parts of solar flares where the emission comes from cool (10^4 K) plasma. This emission is produced mostly in strong resonance lines of hydrogen, calcium or magnesium ($H\alpha$, $H\beta$, $H\delta$, Ca II H , K , etc.) Since the most

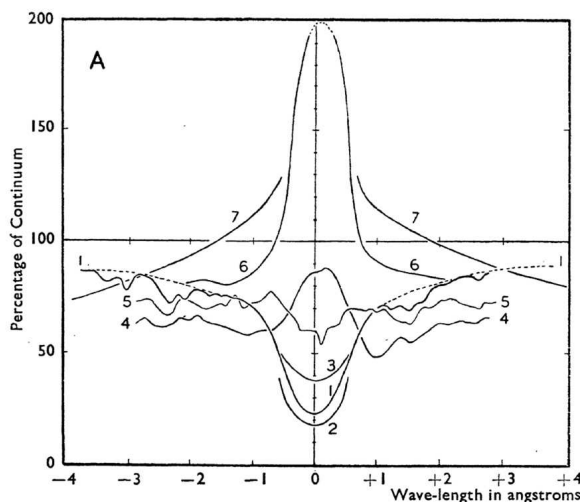


Figure 2. Examples of the observed $H\alpha$ asymmetric line profiles. Profiles 4, 5, and 6 correspond to the flare emission (Ellison 1949).

spectroscopic observations performed during past years concern $H\alpha$ line, the interpretation of these results will take considerable part of this review.

2. Early Observations and Interpretations

Asymmetries of chromospheric lines emitted by the flaring plasma have been observed for more than half of the century. After the solar spectrographs were developed in order to produce the solar spectrum with sufficient spectral resolution, observers noticed that the line profiles emitted during solar flares are not symmetric (Fig. 2). It was clear from the beginning that these kinds of modifications of the spectral lines are due to the mass motion driven during solar flares. However, the mechanisms which could drive the plasma flows were not known yet at those days.

The first analysis of the line asymmetries were concentrated on statistical description of the behaviour of lines. Švestka et al. (1962) presented a qualitative analysis of 244 $H\alpha$ and Ca II K spectra of 92 flares. They found that the blue asymmetry (blue wing enhancement) occurs mainly in the early phase of flares, before flare maximum. However, only 23% of flares contain at least one region with blue asymmetry. 80% of flares exhibit the red asymmetry which dominates during and after the maximum of flare. It is worth to notice that only 5% of flares shows blue asymmetry exclusively. However, because not all flares were observed from their beginning, the occurrence of blue asymmetry may be missed for many flares. In Fig. 3 the time evolution of the asymmetry is presented. Similar analysis was performed by Tang (1983). By inspection of off-band filtergrams of 60 flares obtained in ± 1 and $\pm 2 \text{ \AA}$ from the $H\alpha$ line center he found that 92% of flares show red asymmetry and only 5% show blue asymmetry.

Early statistical analysis gave us an qualitative idea about the line asymmetry but the physical interpretation of the shape of line profiles is not considered.

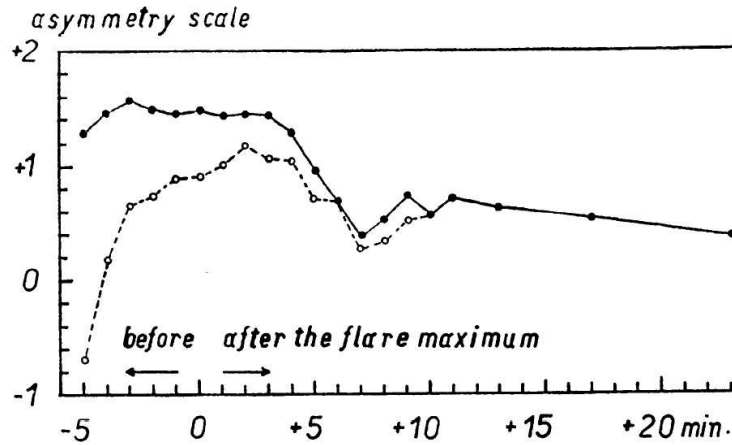


Figure 3. Absolute mean value of the asymmetry of the $H\alpha$ line profiles as a function of time development of flares (solid line). Dashed curve takes positive and negative signs into account. Time of flare maximum = 0 (Švestka et al. 1962).

The asymmetric line profile contains an information about the velocity field in the region where the observed line is formed. Therefore, the first problem which needs to be solved is to determine this velocity field using the observed line profile. Secondly, we have to answer the question why do we observe such a flow of plasma, what can generate the flows?

Determination of the velocity from the observed profiles of the chromospheric lines is not a trivial task due to the complicated processes of line formation and complex velocity field in the chromosphere. Strong chromospheric lines are optically thick and the radiation observed at different parts of the line profile comes from different height z across the chromosphere (Mihalas 1978). The core of strong chromospheric lines (hydrogen Balmer lines, Ca lines) is formed much higher than the wings of these lines. Therefore, the asymmetry of the specific line depends on the relation between the height z of formation of given part of the line profile and the value of the velocity at this height. This means that if the function describing the velocity across the height in the chromosphere is complicated, the emergent line profile has also very complicated shape.

Despite of all difficulties with determining correctly the velocity from the line profile shape, many authors tried to use $H\alpha$, Ca II and other lines to find the velocity in the flaring chromosphere. All these determinations were based on the measurements of Doppler-shifts of the line cores or, more commonly, on the bisector technique.

Using the shift of the line core to obtain the velocity may be misleading and the determined velocity is not correct when the velocity gradient in the chromosphere is significant (Athay 1970). Unfortunately, the estimation of the Doppler-shift obtained with the bisector technique can also give wrong results. The Doppler-shift of the line profile correspond to the shift of the central point of the bisector connecting the two wings of the spectral line. Since the different parts of the spectral line are formed at different height in the chromosphere,

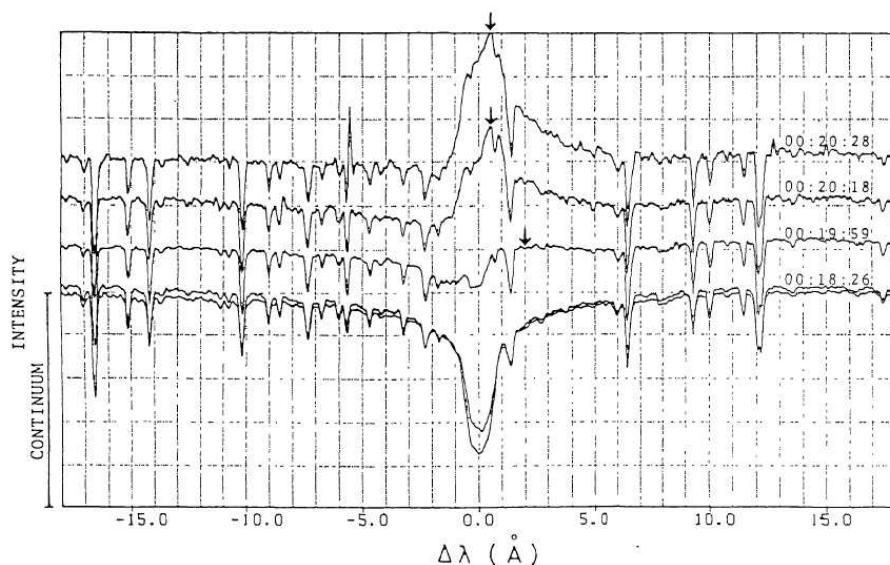


Figure 4. Temporal variation of the H α line profiles observed during solar flare. The black arrow indicates the peak of asymmetric lines. The bottom profile represents the emission of the quiet-Sun area (Ichimoto & Kurokawa 1984).

using bisectors connecting the wings observed at different frequency, we can estimate the line-of-sight velocity at different layers of the chromosphere. However, because the radiation of specific frequency within the spectral line does not come from one narrow layer of the chromosphere but rather from geometrically thick region, we cannot say that the Doppler velocity determined from given bisector correspond to plasma flow at given height in the chromosphere. Moreover, if the velocity gradient in the chromosphere is large then the bisector method cannot be used because the Doppler-shift of any bisector results from a superposition of many shifts due to the motion of plasma with different velocity along line-of-sight. In spite of this the bisector technique was commonly used for many years until it was replaced by more advanced, complicated but much more precise non-LTE radiative transfer techniques with velocity field included.

One of the first interpretation of chromospheric line asymmetry observed during flare was presented by Acton et al. (1982). The authors postulated that these asymmetries are due to chromospheric evaporation driven by accelerated electrons or thermal conduction. Neupert (1968) was probably the first who realise that chromospheric plasma heated during solar flare may evaporate. This evaporated plasma provides material for loop prominences often observed as the so-called post-flare loops (Kopp & Pneuman 1976; Antiochos & Sturrock 1978). For more complete review of chromospheric evaporation see Hudson paper in this book. Acton et al. (1982) postulated that in the analysed flare the non-thermal electrons heat the chromosphere mainly during the impulsive phase, while thermal conduction from the hot coronal plasma heated earlier dominates during the late, thermal phase. Both mechanisms drive upflow of the cool plasma. The

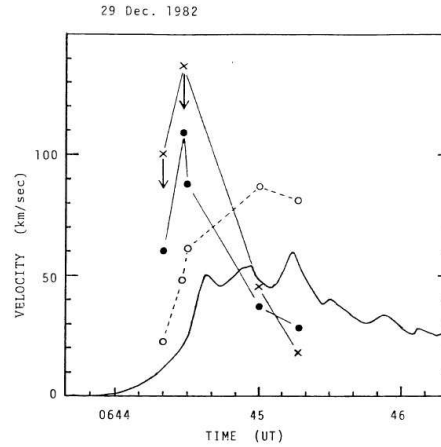


Figure 5. An example of temporal variation of the downflow velocity observed in flaring region. Filled circles correspond to the values obtained from the shift of the $H\alpha$ far wings, while crosses to the values obtained from the shift of the line peak. Open circles represent the time evolution of the $H\alpha$ intensity. The microwave emission at 3750 MHz is also shown (Ichimoto & Kurokawa 1984).

authors stress that for the first time they observed chromospheric evaporation in $H\alpha$ line.

Contradictory results were published by Ichimoto & Kurokawa (1984) who suggested that during the impulsive phase of solar flares the downflow of the cool chromospheric plasma is present. These results are based on the large red asymmetry of the $H\alpha$ line observed during the impulsive phase of many solar flares (Fig. 4). The downward motion increases at the onset of a flare to its maximum velocity of 40 to 100 km s^{-1} shortly before the impulsive peak of microwave emission, and rapidly decreases before the $H\alpha$ reaches its maximum (Fig. 5). The red asymmetry of the $H\alpha$ line may be also explained by the attenuation of the blue wing by the rising plasma over the flare but the authors exclude this case because the optical thickness of a rising cloud is too small to explain the emission deficit of the blue wing of $H\alpha$ line. Also the high temporal resolution spectroscopic observations of $H\alpha$ line performed by Wuelser (1987) confirm the existence of red asymmetry during the impulsive phase of solar flares. The largest asymmetry is observed during the maximum of microwave emission what confirms the earlier results that the plasma downflow is driven by the accelerated non-thermal electrons.

3. Hydrodynamic Modeling of the Flows

The downflow of cool plasma in the form of chromospheric condensations observed during solar flares was predicted theoretically by Fisher et al. (1985a). If a region of the chromosphere heated by non-thermal electrons is thick enough, then the rapid temperature increase produces an enhanced pressure in the heated region. This overpressure, besides the evaporation, also drives downward moving

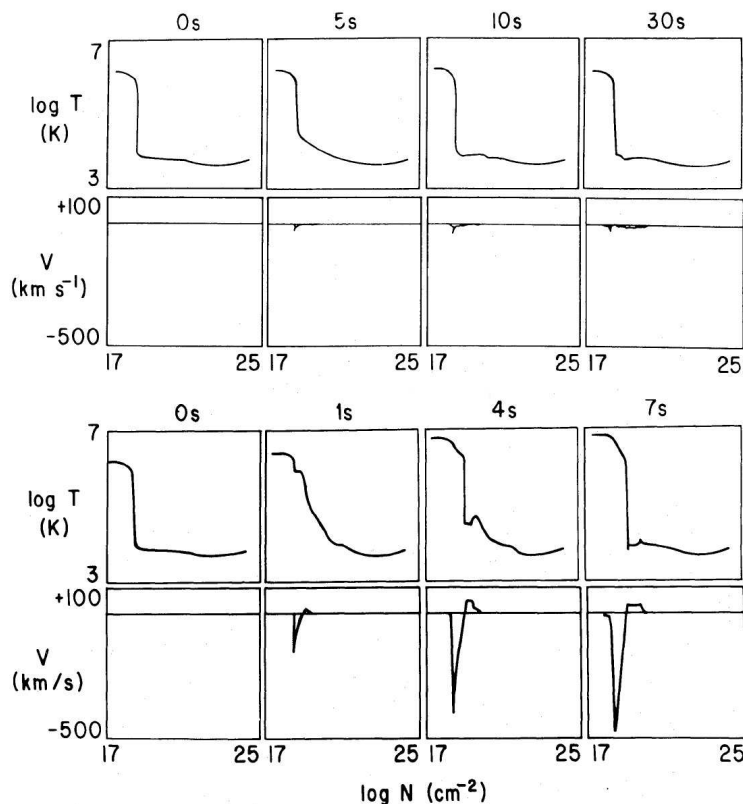


Figure 6. Time evolution of the temperature and velocity in the loop atmosphere heated by the low (upper two panels) and the high (lower two panels) flux of non-thermal electrons. In the first case the upflow with the low velocity in the transition region and in the chromosphere is present (gentle evaporation). For the strong flux of non-thermal electrons the high-velocity upflow (up to -500 km s^{-1}) in the high temperature region is obtained (explosive evaporation) and downflow (up to $+40 \text{ km s}^{-1}$) is observed in the chromosphere (chromospheric condensations). For more details see the paper of Fisher et al. (1985a).

cool and dense chromospheric condensations (Fisher et al. 1985b) which seem to be responsible for red asymmetry of the $\text{H}\alpha$ line profiles reported by many authors. Fisher et al. (1985b) modeled the hydrodynamic and radiative response of the atmosphere to short impulsive injections of non-thermal electron beams (Fig. 6). They showed that a high-energy flux of non-thermal electrons drives explosive evaporation accompanied by the formation of cool chromospheric condensations in the flare chromosphere. A different situation occurs when the flux associated with non-thermal electrons is very low. Then only a weak chromospheric evaporation takes place. This kind of evaporation is referred to as gentle evaporation (Antiochos & Sturrock 1978; Schmieder et al. 1987) and it can be observed in chromospheric spectral lines like $\text{H}\alpha$ or in $\text{Ca II } 8542 \text{ \AA}$. Antiochos & Sturrock (1978) suggested that the gentle chromospheric evaporation may also occur after the primary energy release, when the non-thermal

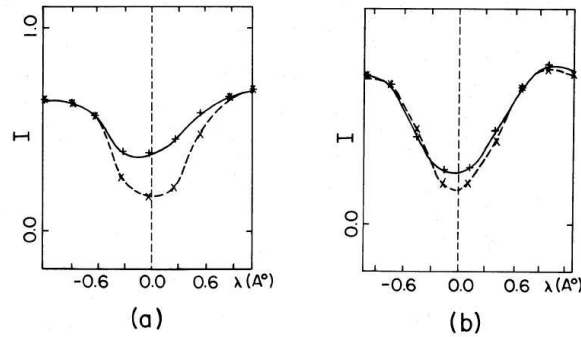


Figure 7. $H\alpha$ line profiles observed during the gradual phase of a solar flare (solid lines). Weak blue-shift of these lines suggests slight upflow of the plasma with the velocity of a few km s^{-1} interpreted as gentle evaporation. Dashed lines represent the reference line profiles of the quiet Sun area (Schmieder et al. 1987).

electron flux is stopped. This evaporation could be driven by the large conductive heat flux from a high temperature flare plasma contained in magnetic tubes above the chromosphere. Such physical conditions may appear during the gradual phase of solar flares, when there is no significant flux of non-thermal electrons. In the Forbes et al. (1989) model for flare-loop formation by magnetic reconnection the conduction of the thermal energy generated at the slow-mode shocks drives a gentle evaporative upflow from the ribbons.

Schmieder et al. (1987) observed small but long-lasting blue-shifts in flare ribbons in the $H\alpha$ line during the gradual phase of three solar flares and interpreted them as due to upflows with velocities less than 10 km s^{-1} (Fig. 7). These upflows were believed to be caused by gentle chromospheric evaporation driven by the heat conduction along the field lines connecting the chromosphere with a reconnection site in the corona.

The downflow of cool chromospheric plasma during the impulsive phase of solar flares predicted in the theoretical calculations was reported by many authors. Zarro et al. (1988) observed large red asymmetry of the $H\alpha$ line during the period of hard X-ray burst (Fig. 8). These asymmetries were used to determine the downward velocities estimated from the maximum shift of the centroid of the bisectors. The averaged over all red-shifted pixels during the impulsive phase velocity was of the order of $60 \pm 10 \text{ km s}^{-1}$. The downflow analysed in the $H\alpha$ data and the upflow observed in the X-ray lines allows the authors to analyze the momentum balance of the flow. They conclude that the momenta of upflowing and downflowing plasma are approximately equal. Zarro & Canfield (1989) conclude that the downflow velocity measured from red wing enhancement can be used as a diagnostics of impulsive solar flare heating conditions (Fig. 9).

The work of Ding et al. (1995) shows that the velocity of chromospheric downflows deduced from the red asymmetry of $H\alpha$ line is around $30 - 40 \text{ km s}^{-1}$ with the lifetime of the order of 2 – 3 minutes. There are two major problems found by the authors: Why is the line center nearly not shifted while the line wing shows great asymmetries? The second problem concerns the life time of

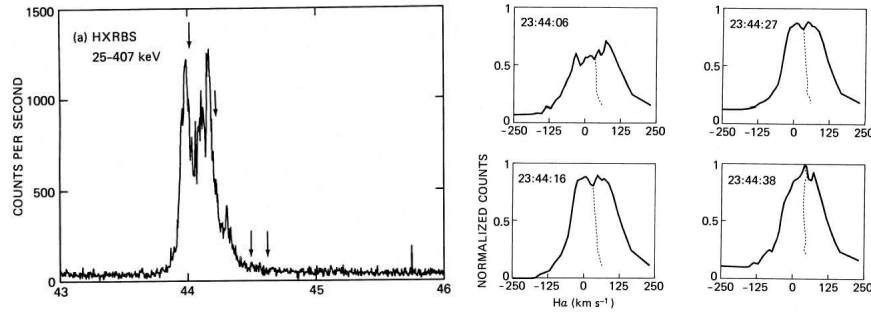


Figure 8. The hard X-ray emission (left) and the $H\alpha$ excess line profiles (right) observed during the impulsive phase of a solar flare. Dashed lines mark the centroids of the profile. The obtained downward velocities are around 50 km s^{-1} . The numbers on the X-axis of left panel represent minutes after 23 UT and the arrows – the times of $H\alpha$ observed line profiles (Zarro et al. 1988).

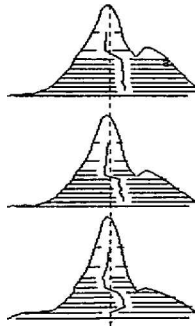


Figure 9. An example of the $H\alpha$ line profiles observed during the impulsive phase of a solar flare. The red wing enhancement is observed at the same time as strong hard X-ray emission. Note that the central part of the line is slightly blue-shifted (Zarro & Canfield 1989).

the downflow which is considerably longer than the life time predicted in Fisher (1989) simulations. Recent hydrodynamic and radiative transfer simulations may now explain these two problems.

There are more papers presenting the observations of the red asymmetry related to the chromospheric condensations driven during the impulsive phase of solar flares (e.g., Wuelser & Marti (1989) – Fig. 10). All of them determine more or less consistent observational picture of the chromospheric flows during the impulsive phase of flares. This picture is based on many spectroscopic observations of the chromospheric line profiles. An important step was done when it became possible to calculate theoretical line profiles and compare them with observations.

Canfield & Gayley (1987) computed time-dependent $H\alpha$ line profiles for the dynamic model atmosphere of Fisher et al. (1985a). They simulate the effects of power-law electron beam heated chromosphere. Solving the radiative transfer equations for one-dimensional model atmosphere the evolution of $H\alpha$ line profile was estimated. The time of the electron beam heating was 5 s and for detailed de-

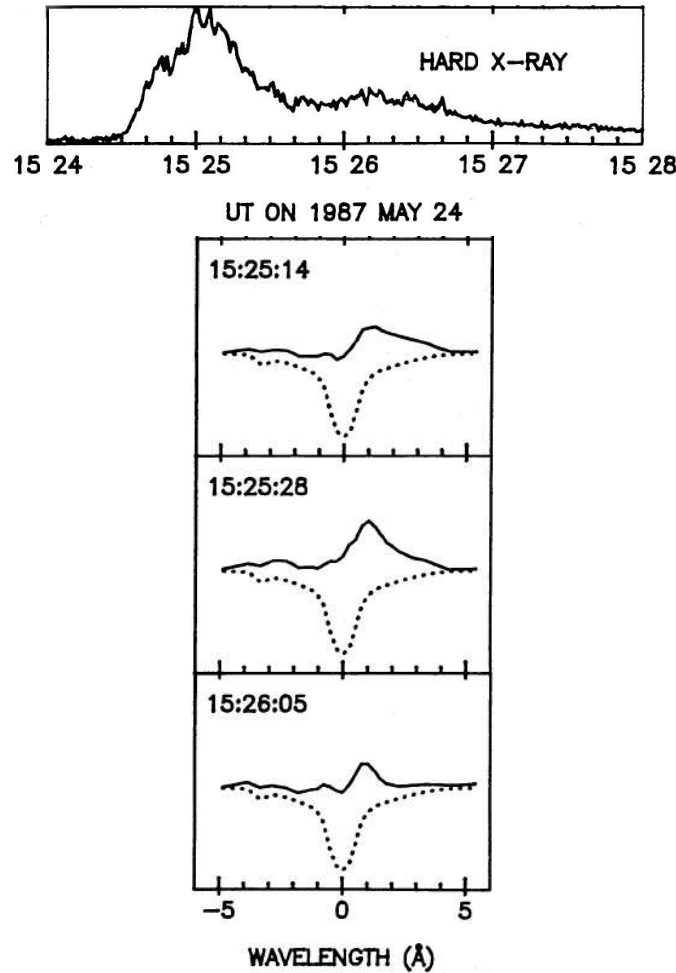


Figure 10. The hard X-ray emission (top) and the H α line profiles with the red asymmetry (bottom) observed during the impulsive phase of a solar flare. Dotted lines mark the reference quiet Sun profile (Wuelser & Marti 1989).

scription of other parameters and computational methods see Canfield & Gayley (1987). In Fig. 11 the time sequence of the H α line profile is presented. During the non-thermal heating, the red-shifted component is present but after the heating was stopped, the H α line exhibit the blue asymmetry although the central absorption feature is shifted towards longer wavelengths. This behaviour is explained by downflow of the chromospheric condensation. It is also worth to notice that the response of the H α emission to the non-thermal electron beam is very fast (less than second).

Similar but more precise simulations of the dynamics and radiation in a solar flare loop was presented by Abbett & Hawley (1999). Except the non-thermal heating of the chromosphere, they took into account the thermal heating by the soft X-ray irradiation within 1 – 250 Å range. Carlsson & Stein (1997) radiative-

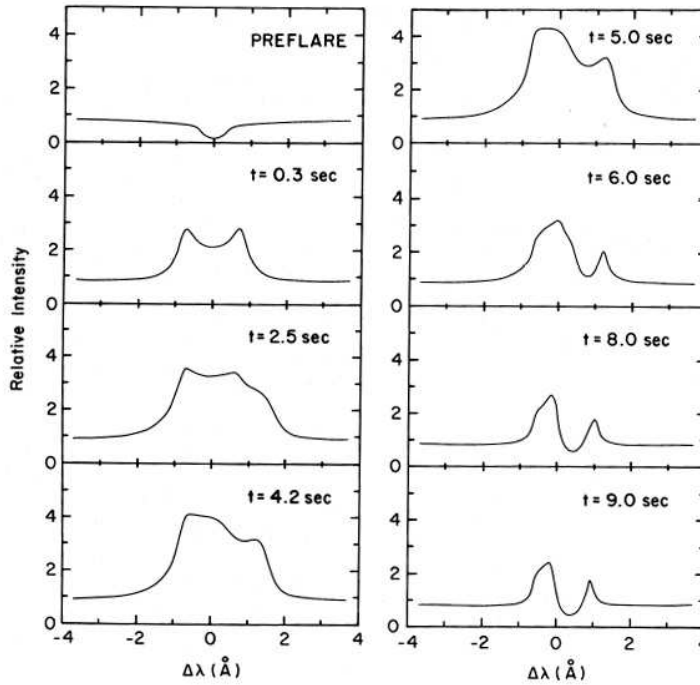


Figure 11. Time evolution of the calculated $H\alpha$ line profiles for the electron beam heated model atmosphere of Fisher et al. (1985a) (Canfield & Gayley 1987).

hydrodynamic code was used to analyze the response of the lower atmosphere at the footpoint of a flare loop. In the radiative transfer calculations the important transitions of hydrogen, helium and singly ionized calcium and magnesium were treated in non-LTE. One-dimensional atmospheric model was used in the calculations.

As a starting models the authors took two different cases PF1 and PF2. The temperature and electron density stratifications of both preflare atmospheres are shown in Fig. 12. Three levels of the non-thermal heating was considered which correspond to weak (F9), moderate (F10), and strong (F11) non-thermal flare heating. The PF1 atmosphere is heated for 70 s with the F9 and F10 fluxes, and the PF2 atmosphere is heated for a shorter, 4 s burst but with strong F11 heating.

Figure 13 presents the time evolution of emergent $H\alpha$ and $Ca II K$ line profiles. For the $H\alpha$ line separated blue-shifted component is clearly visible while $Ca II$ line exhibit red-shifted component. The contribution function calculated for these two lines explain why we observe such a two-components and asymmetric profiles (Fig. 14).

This analysis shows that the evolution of non-thermally heated chromosphere progresses through two distinct dynamic phases (Abbett & Hawley 1999): a gentle phase, where the non-thermal energy input of the flare is essentially radiated away into space, and an explosive phase, where the flare energy rapidly

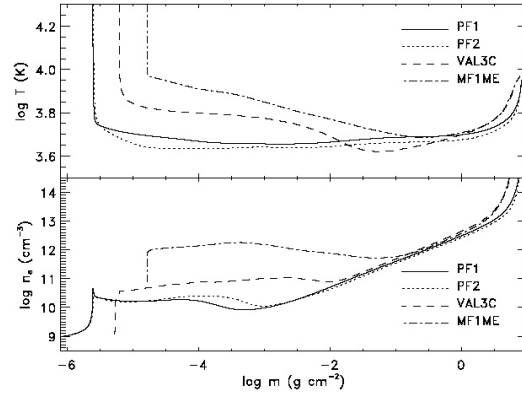


Figure 12. The temperature and electron density stratifications of both preflare atmospheres PF1 and PF2 compared to the standard semiempirical VAL3C chromospheric model of Vernazza et al. (1981) and to the semiempirical active atmosphere MF1ME of Metcalf (1990) (Abbett & Hawley 1999).

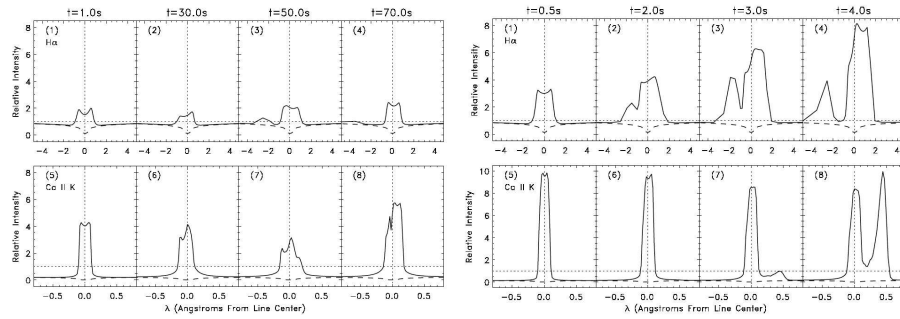


Figure 13. *Left:* Time evolution of the H α and Ca II K line profiles for moderate heating of the atmosphere by non-thermal electrons (model F10). In each panel, the vertical axis represents relative intensity with respect to the continuum level and the horizontal axis denotes the wavelength from the line centre. The dashed lines in each panel represent the preflare line profile. *Right:* Time evolution of the H α and Ca II K line profiles but calculated for strongly heated atmosphere (model F11) (Abbett & Hawley 1999).

heats the atmosphere and drive large amounts of chromospheric material up into the corona, and down toward the photosphere. During the explosive phase, there is significant plasma motion and there are steep velocity gradients. Moreover, the effects of thermal X-ray heating of the chromosphere remain negligible compared to the non-thermal heating in the impulsive phase.

Similar, but much more extended calculations were presented by Allred et al. (2005). The basics of computational methods are similar to those described by Abbett & Hawley (1999) but there are some significant improvements. The authors include the double power-law electron beam energy distributions recently observed in solar flares with the Reuven Ramaty High-Energy Solar Spectroscopic Imager (RHESSI) satellite. Additionally, the effects of XEUV heating from a large number of high-temperature lines was taken into account using

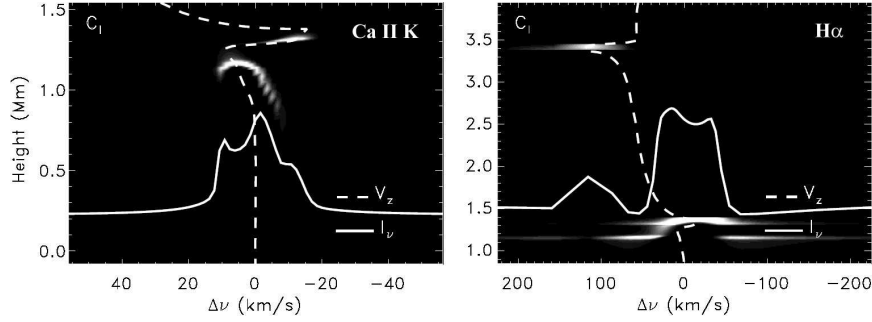


Figure 14. The approximate formation height of different parts of the spectral line profile may be described by contribution function. This figure presents components of the intensity contribution function for Ca II K (left) and H α (right) lines after 50 s of flare heating in model F10. Line frequencies are in velocity units. Atmospheric velocities (dashed lines) are taken to be positive toward the corona. Thus, negative velocities associated with downward-moving material correspond to red-shifts in the profile (Abbett & Hawley 1999).

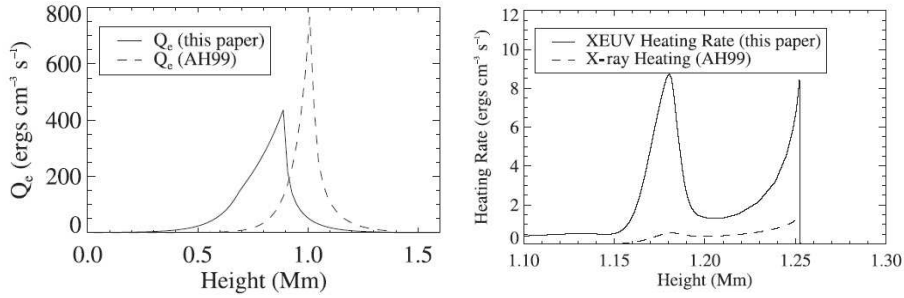


Figure 15. *Left:* Comparison of the electron beam heating rate in the pre-flare atmosphere for the F10 flare model. The solid line shows the heating rate used in the paper of Allred et al. (2005), and the dashed line shows the initial beam heating rate of Abbett & Hawley (1999). *Right:* Solid line – thermal XEUV heating used in Allred et al. (2005), dashed line – soft X-ray heating rate used previously by Abbett & Hawley (1999).

results from the CHIANTI and ATOMDB databases and a wide range 1 – 2500 Å was used for direct thermal heating of the chromosphere. Figure 15 present the comparison of the heating rates used by Abbett & Hawley (1999) and Allred et al. (2005).

These new calculations confirmed the previous results. However, the line profiles evolution differs from the Abbett & Hawley (1999) calculations – the line asymmetry is not so significant and the blue and red components of the H α and Ca II K lines, respectively, are not observed separately. Instead, the lines are asymmetric with blue or red wing enhancement (Fig. 16). As in Abbett & Hawley (1999), the authors found that the impulsive flare naturally divides into two phases, an initial gentle phase followed by a period of explosive increases in temperature, pressure and velocity.

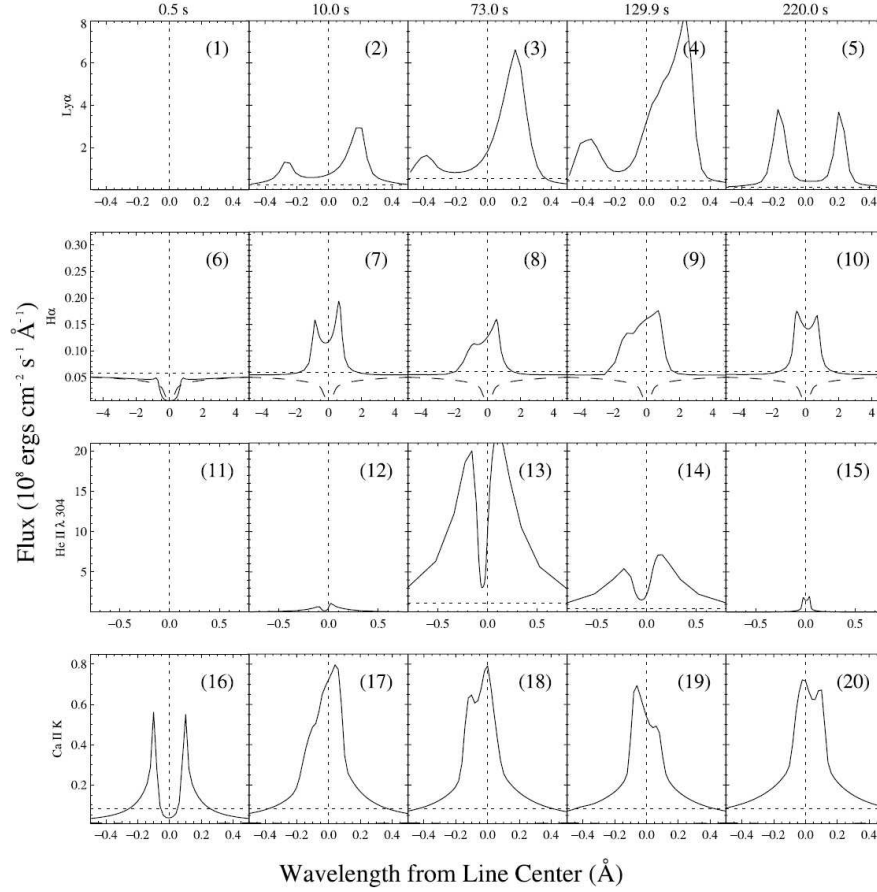


Figure 16. Time evolution of the synthetic line profiles of Ly- α , H α , He II 304 Å, and Ca II K lines for the moderate level of non-thermal heating (model F10). Times are indicated at the top of each column. The dotted lines indicate the level of the continuum close to the line center, while the dashed line is the preflare line profile (Allred et al. 2005).

There are more papers which treat the problem of plasma flows in the non-thermally heated chromosphere (Mariska et al. 1989; Emslie et al. 1998; Karlický & Hénoux 1992; Gan & Fang 1990; Gan et al. 1991). All these hydrodynamic simulations predict an upflow of the hot coronal plasma due to the enhanced pressure in the region heated by non-thermal electrons or protons. This upflow is associated with downflow of chromospheric condensations, but with much lower velocities (Fig. 17). These condensations disturb the line profiles emitted from the chromosphere and cause significant asymmetries observed e.g., in H α line.

The calculated line profiles emerging from flaring atmosphere show roughly similar behaviour than the observed ones but unfortunately, the appearance and the time evolution of the calculated line profiles was not compared to the spectroscopic observations of particular flares. The validity of the modeling summarized in this chapter was not confirmed observationally up to now.

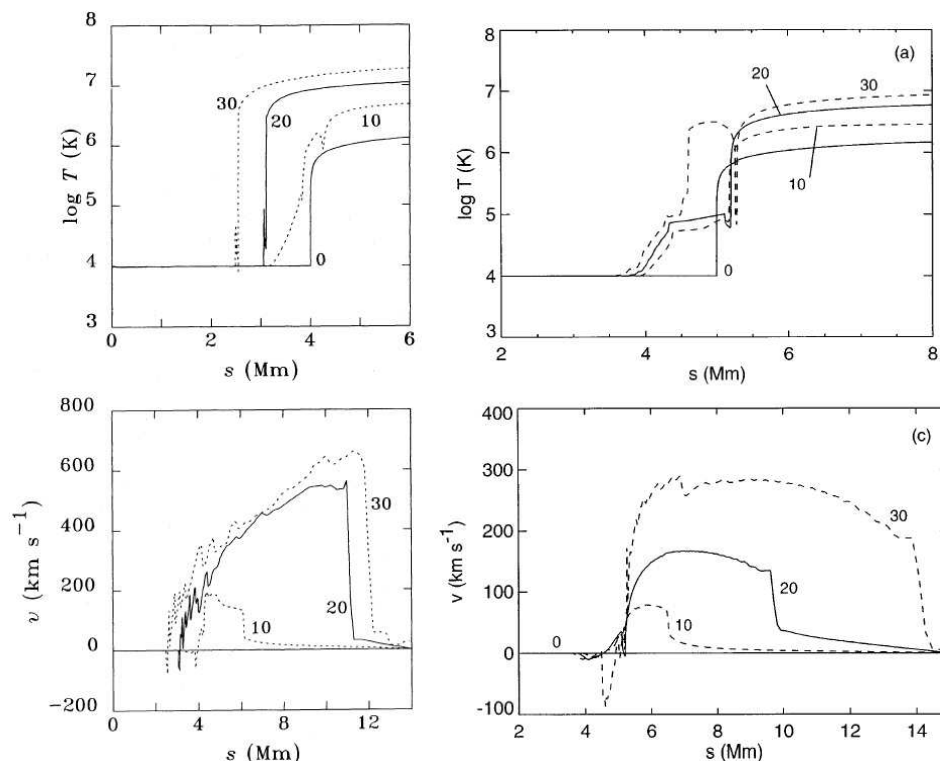


Figure 17. Left panels: Hydrodynamic response of the temperature and velocity to the non-thermal electron beam heating (Mariska et al. 1989) and to the non-thermal proton beam heating (right panels) (Emslie et al. 1998). Positive values of the velocity correspond to upward motion of the plasma. Labels 10, 20, and 30 are the times in seconds after start of non-thermal heating.

4. Velocity Field in Semiempirical Models of the Flare Atmosphere

Asymmetries observed in chromospheric line profiles are also modeled using semiempirical flare models. This approach is based on the idea that the temperature stratification of the atmosphere is determined empirically in the way to reproduce the calculated spectrum in the best agreement with observations. This means that the energy-balance equation is not considered. Many spectral lines and continua are used to construct such kind of models. Initially, static semiempirical models were developed for a quiet-Sun atmosphere (Vernazza et al. 1981) and then for the static flaring atmosphere (Machado et al. 1980). These models were constructed under assumption of 1-dimensional geometry and hydrostatic equilibrium (Fig. 18). They are static however the time sequence of many semiempirical models can be used to describe the evolving atmosphere but this method is valid only for slowly-evolving atmospheres. More detailed description of semiempirical models can be found in the paper of Mauas in this book.

Non-LTE radiative transfer methods applied to semiempirical models allows us to calculate the spectrum emerging from the atmosphere. In particular,

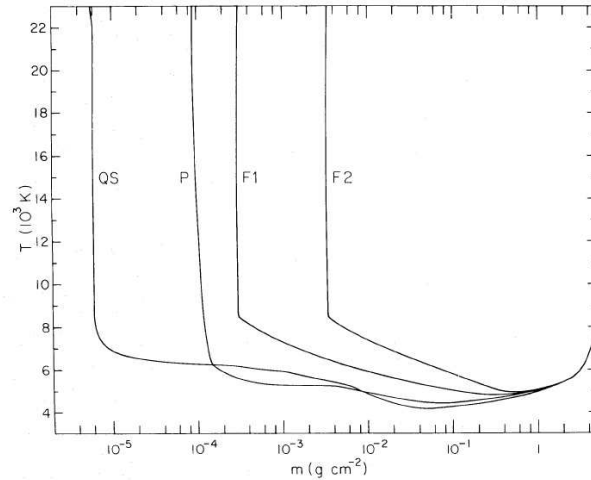


Figure 18. Temperature as a function of column mass for the flare models F1 and F2, for the quiet-Sun QS (VAL-C) model of Vernazza et al. (1981) and for the plage (P) model of Basri et al. (1979) (from Machado et al. 1980).

the profiles of the chromospheric optically thick lines may be calculated in details (Heinzel et al. 1994). It is also possible to reproduce asymmetric line profiles solving the transfer equation for a dynamic atmosphere with velocity field, using previously calculated level populations for static model (Berlicki et al. 2005). However, this approach is justified only for relatively small velocities ($V \leq 10 \text{ km s}^{-1}$) which do not significantly affect the level populations of the static model (Nejezhleba 1998). It cannot be used for impulsive phase of flares to model the chromospheric condensations which move quite fast. Therefore, such simplified calculations are used to model e.g., the gradual phase of solar flares, when the velocities in the chromosphere are low.

One of the first semiempirical modeling of chromospheric flows was performed by Gan et al. (1993). Using the $H\alpha$ line profiles observed for two flares the authors constructed the series of semiempirical models with chromospheric condensations. It was shown that chromospheric condensations are responsible not only for the red asymmetry of the $H\alpha$ line, but also for the blue asymmetry of the line with central reversal (Fig. 19). Chromospheric condensations were assumed to be homogeneous with constant velocity. The most important conclusion of this paper is that the properties of chromospheric condensations seem to be consistent with the results of hydrodynamical models of solar flares. Comparison of calculated $H\alpha$ line profiles with real observations present also a valuable part of this paper.

An interesting work was presented by Nejezhleba (1998) who simulate the influence of the velocity field on the $H\alpha$ line profiles. The calculations were performed using non-LTE model of plane-parallel solar flare atmosphere with stationary velocity field. This velocity field was applied to different layers of the solar atmosphere and the emergent $H\alpha$ line profiles were calculated for two models of solar flare F1 and F2 (Machado et al. 1980). Figure 20 present an example of asymmetric line profiles calculated for a weak-flare model atmosphere F1 and

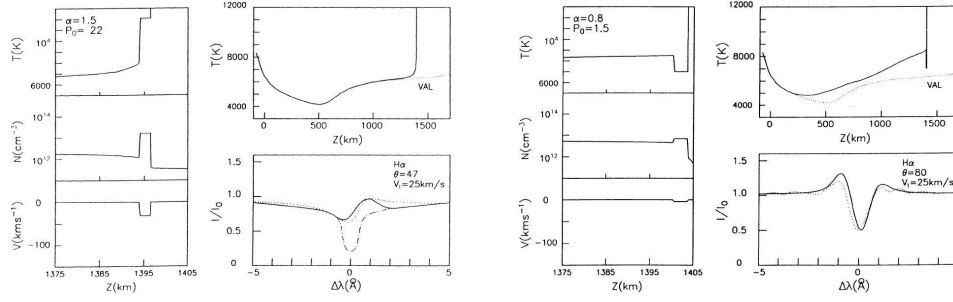


Figure 19. Two examples of semiempirical models of the chromosphere with cool condensation. Left three panels correspond to the condensation which is responsible for the red asymmetry of the $H\alpha$ line while right three panels presents condensation producing $H\alpha$ line with blue asymmetry. Temperature, electron density and velocity stratification is presented for both cases (negative sign of the velocity corresponds to downflow). The calculated $H\alpha$ line profiles are plotted with solid line, observed ones – with dotted line (Gan et al. 1993).

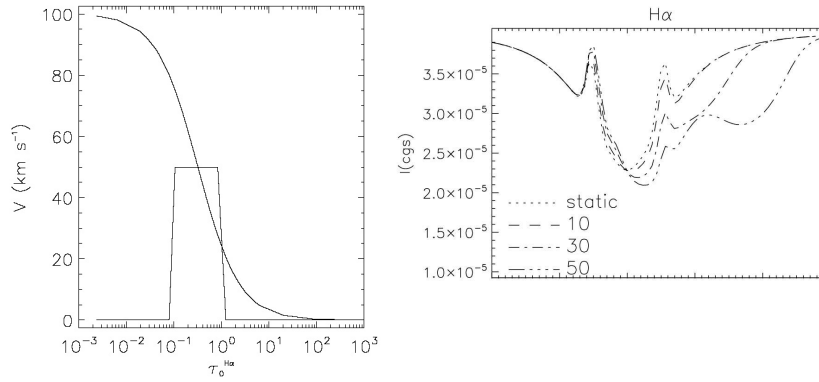


Figure 20. *Left:* Models of the velocity field in the chromosphere used in the non-LTE calculations (positive sign of the velocity corresponds to downflow). *Right:* Some examples of synthetic $H\alpha$ line profiles calculated for a static and dynamic atmosphere with different velocities 10, 30, and 50 km s^{-1} (Nejezhleba 1998).

for different velocity fields. The main conclusion of this work is that the velocity field affects the level populations via the increase of the downward radiation. Nevertheless, for velocities that do not exceed the thermal velocity of plasma, one can use the static populations for the formal solution of radiative transfer equation including the velocity to reproduce the observed line asymmetries. Other important point is that application of the bisector method would lead in some cases to reverse velocity, in others to underestimation of the velocity. It includes, besides the part of the profile directly affected by the moving material, also a “static” part of the profile. To use the bisector in terms of Doppler-shift the static part should be somehow eliminated. This remark makes questionable all estimations of the Doppler velocity obtained with the bisector method applied to self-reversed or emission chromospheric lines observed in solar flares.

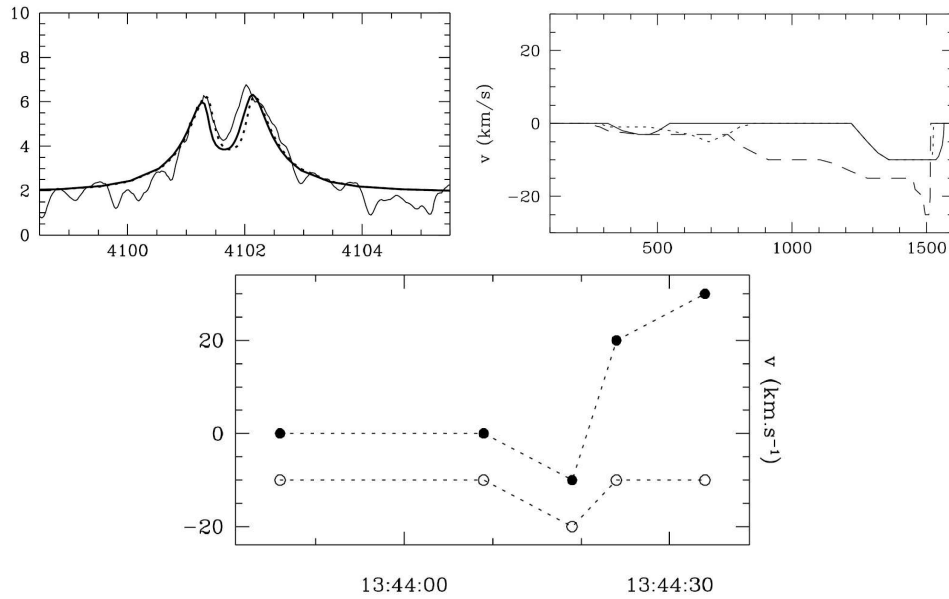


Figure 21. An example of the observed (thin line) and fitted (thick line) H δ line profiles and determined velocity field across the atmosphere. Negative value indicates an upward velocity. In the lower panel the time evolution of the velocity value at two different heights in the atmosphere is presented. Filled circles refer to the height ≈ 900 and open circles to the height ≈ 1400 km (Falchi & Mauas 2002).

The conclusions of Nejezhleba (1998) suggest that deducing the velocity from flare line profiles is rather difficult and cannot be done only by searching for Doppler-shifts with the bisector method. Chromospheric line profiles suggest that the flare atmosphere is highly dynamic and stratified with rather complicated plasma motion. These lines are optically “thick” and the only reliable way to analyze the flows is to use the non-LTE radiative transfer codes, which enable us to compute the chromospheric models with velocity fields. Resulting synthetic line profiles can then be compared with the observed ones.

The direct comparison of the observed and synthetic line profiles was presented in the paper of Falchi & Mauas (2002). They study the chromospheric structure of a small flare and construct 5 semiempirical models for different times, which reproduce the profiles of the H δ , Ca II K, and Si I 3905 Å lines during the flare evolution. In order to reproduce the asymmetry of the lines the velocity fields were introduced in the line profile calculations. The modeling was done using the non-LTE Pandora code of Avrett & Loeser (1984). The trial-and-error method was used to reproduce the observed line profiles by the synthetic ones. Figure 21 (upper panels) present an example of the observed and fitted H δ line profiles and determined velocity field across the atmosphere. In the lower panel of Fig. 21 the time evolution of the velocity value at two different heights in the atmosphere is presented. The presence of an upward motion in the flaring atmosphere at 1400 km, might be a signature of the chromospheric evaporation observed at chromospheric levels. It is interesting to notice that around 13:44:30

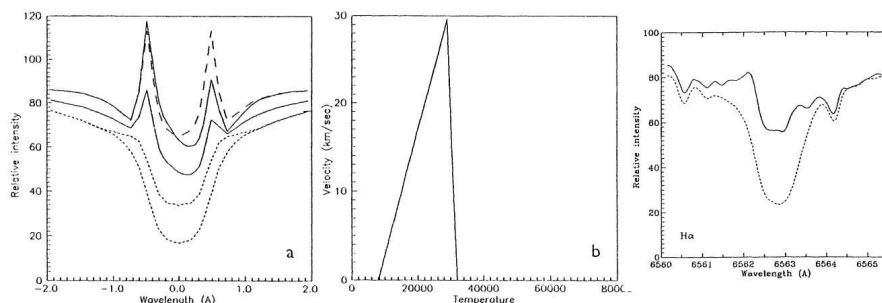


Figure 22. Left: Simulation of the influence of the downward velocity field on the emergent $H\alpha$ line profile emitted from flaring model atmosphere F1 of Machado et al. (1980). In the middle panel the velocity used in the modeling as a function of temperature is shown (positive sign of the velocity indicates downflow). Also an example of the observed $H\alpha$ line with red asymmetry is presented (for details see Heinzel et al. (1994)).

UT the downflow is observed at the height of 900 km, while the upward motion is evident at 1400 km above the photosphere. One possible explanation is that chromospheric evaporation together with condensations is observed. In this case chromospheric evaporation is observed at chromospheric levels and not, as more common, at coronal levels.

Using the semiempirical F1 model of a weak flare (Machado et al. 1980), Heinzel et al. (1994) showed that the blue asymmetry of $H\alpha$ line profile is observed due to the downflow of chromospheric plasma. It is interesting to notice that the blue asymmetry is associated with the red-shift of the central absorption feature. Similar results was shown by Gan et al. (1993). The structure of the velocity field used in the non-LTE simulations of Heinzel et al. (1994) was qualitatively consistent with the concept of downward-moving chromospheric condensations (Fig. 22). These calculations were performed using the non-LTE code developed by Heinzel (1995) and modified for flare conditions. The code uses a 1D plane-parallel geometry and the atmosphere is in hydrostatic equilibrium. Hydrogen excitation and ionization equilibrium have been computed by solving simultaneously the radiative transfer equations, the equations of statistical equilibrium for a five-level plus continuum atomic model of hydrogen and the equations of particle and charge conservation. The equations of statistical equilibrium have been preconditioned according to Rybicki & Hummer (1991). The preconditioning is based on the lambda-operator splitting technique, where the exact lambda operator is expressed as an approximate operator plus the correction. Then the correction is iteratively applied to a lagged source function by using the so-called Accelerated Lambda Iterations (ALI) method. For multilevel atoms this method is referred to as MALI – Multilevel Accelerated Lambda Iterations (Rybicki & Hummer 1991). The preconditioned equations are then linearized with respect to the atomic level populations and electron density and solved iteratively (Heinzel 1995).

This non-LTE code was also used in Berlicki et al. (2005) to analyse the time evolution of the line asymmetry observed during the gradual phase of the solar flare on October 22, 2002. In this paper for the first time the evaporative flows

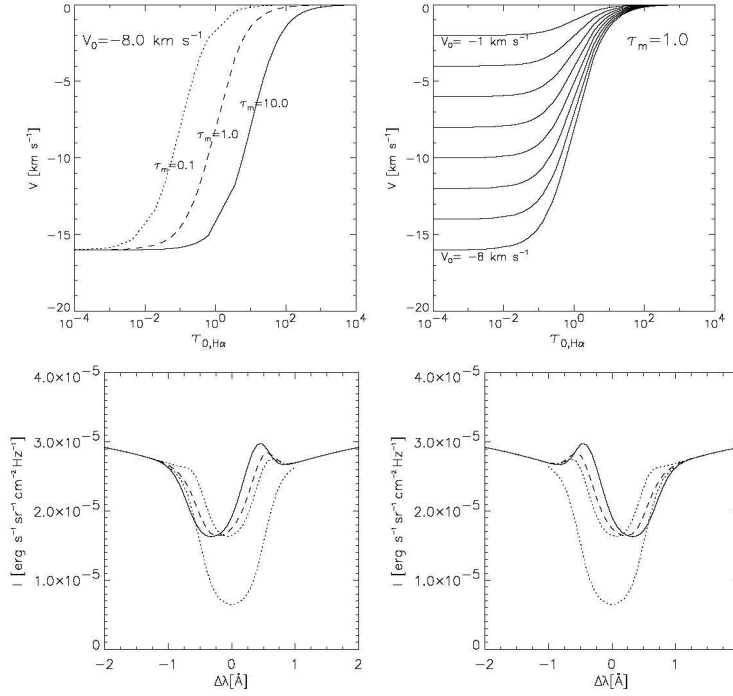


Figure 23. The H α line-centre optical depth distribution of the velocity field used in the modeling plotted for different values of τ_m and for $V_0 = -8 \text{ km s}^{-1}$ (upper left panel) and for different values of V_0 and for $\tau_m = 1.0$ (upper right panel). In the lower panels the influence of the velocity field on H α line profiles emitted from flare is presented (upflow defined by $V_0 = -8$ and downflow $V_0 = +8 \text{ km s}^{-1}$ for three values of $\log \tau_m = 0.1, 1.0$, and 10.0 (dotted, dashed and continuous lines, respectively) (Berlicki et al. 2005).

in the gradual phase are studied quantitatively by using a non-LTE radiative transfer code and spectroscopic observations of the flare ribbons. First the authors analyse the influence of different velocity fields on the emergent H α line profile. Again, it was shown that the downflow of flaring plasma causes blue asymmetry of the self-reversed line while upflow – red-asymmetry (Fig. 23). For the modeling of the observed line asymmetry except the changes of the value of the velocity, also the height of the velocity field in the atmosphere was different. The procedure of fitting the H α line profiles was performed using a grid of many models by varying different parameters. Each observed profile was fitted by the least-square technique to a closest synthetic profile from the grid and the model with the velocity field was found for each analysed line profile.

In the analysis the MSDP (Multichannel Subtractive Double Pass) spectrograph (Mein 1991) coupled to the VTT telescope working at the Teide Observatory (Tenerife, Canary Islands) was used. 36 H α line profiles (six areas at six different times) observed during the M1.0 flare on October 22, 2002 were taken for the analysis (Fig. 24 – upper left panel). As an example we present in Fig. 24 (lower panel) some profiles observed in chosen area at three times. These observed profiles (solid lines) are fitted with the synthetic ones (dashed lines)

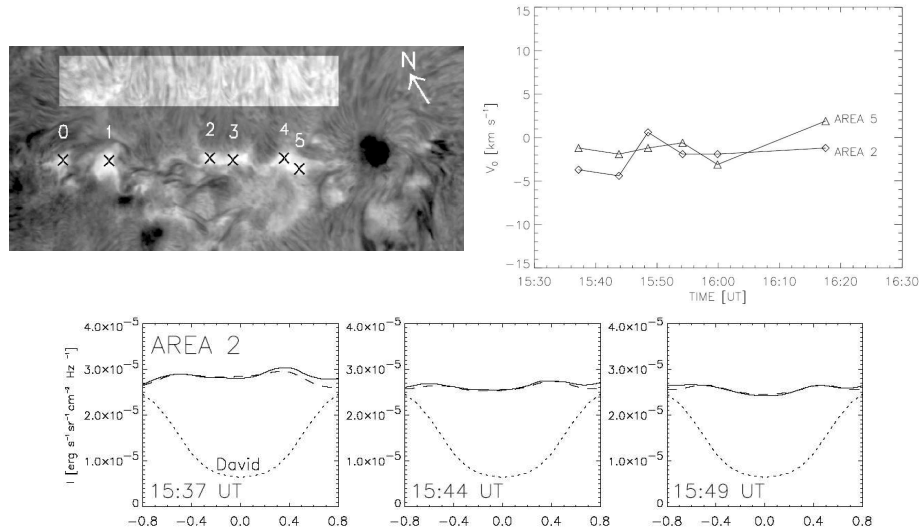


Figure 24. The image of the flare on October 22, 2002 used in the analysis of Berlicki et al. (2005) and the observed (continuous lines) and fitted (dashed lines) $H\alpha$ line profiles (upper and lower left panels). 0 – 5 are the areas used in the analysis. The time evolution of the velocity in the chromosphere deduced from line asymmetries is plotted for two analysed areas in the right panel. Negative velocities correspond to upflow (Berlicki et al. 2005).

obtained from the grid. In the right panel of Fig. 24 the temporal evolution of the velocity field is presented for two different areas of the flare.

The authors interpret the upflows found in the flare ribbons in terms of the Antiochos & Sturrock (1978) model for gentle evaporation. This process may occur during the gradual phase of solar flares and it can be driven by conductive heat flux from the high-temperature flare plasma contained in magnetic flux tubes above the photosphere. In the future it would be interesting to use more spatial points at more times and to use the spectra obtained within a wider range of wavelengths. Other distributions of the velocity field in the chromosphere should also be tested. In addition, to perform non-LTE modeling of the flare structure it would be useful to have other spectral lines formed at different levels of the chromosphere.

5. Summary

In this review I presented some interesting papers concerning plasma flows observed during solar flares in cool chromospheric layers. These flows are directly responsible for the line-asymmetries and/or line-shifts often observed in chromospheric lines emitted by the flaring plasma.

An important work was done to understand the flows and their mechanisms. In order to determine the plasma velocity and flow direction the bisector method

was applied for line profiles. Unfortunately, as we could see, this method leads in some cases to misleading estimations of the velocity. Recently, the direct comparison of the observed and synthetic line profiles gives more valuable information about velocity fields in the chromosphere. All the data support the evaporative model of solar flares where explosive chromospheric evaporation of the hot plasma is associated with the chromospheric condensations observed in “cool” chromospheric lines. In the late phases of flares the gentle evaporation may be observed in chromospheric lines.

For the future it is necessary to use large and dense grids of the chromospheric models computed with hydrodynamic and non-LTE codes. They may help us to understand the flows and give more realistic description of the physical processes during the flares, particularly the heating mechanisms and their role at different phases of the flare evolution.

Finally, really good spectral observations of flares are needed. They have to be co-spatial, simultaneous and obtained in different spectral ranges (X-ray, EUV, UV, optical, IR). Such observations would be very helpful to construct the full picture of the plasma flows during flares. There are some data concerning the flows observed in soft X-ray and EUV but they are extremely rare and almost never co-spatial nor simultaneous with the observations in chromospheric lines.

Acknowledgments. This research was supported by the European Commission through the RTN programme (European Solar Magnetism Network, contract HPRN-CT-2002-00313. The author also would like to thank P. Heinzel for helpful comments and valuable remarks.

References

- Abbett W. P., Hawley S. L., 1999, *ApJ* 521, 906
 Acton L. W., Leibacher J. W., Canfield R. C., Gunkler T. A., Hudson H. S., Kiplinger A. L., 1982, *ApJ* 263, 409
 Allred J. C., Hawley S. L., Abbett W. P., Carlsson M., 2005, *ApJ* 630, 573
 Antiochos S. K., Sturrock P. A., 1978, *ApJ* 220, 1137
 Athay R. G., 1970, *Solar Phys.* 12, 175
 Avrett E. H., Loeser R., 1984, Line transfer in static and expanding spherical atmospheres, 341–379, *Methods in Radiative Transfer*
 Basri G. S., Linsky J. L., Bartoe J.-D. F., Brueckner G., van Hoosier M. E., 1979, *ApJ* 230, 924
 Berlicki A., Heinzel P., Schmieder B., Mein P., Mein N., 2005, *A&A* 430, 679
 Canfield R. C., Gayley K. G., 1987, *ApJ* 322, 999
 Carlsson M., Stein R. F., 1997, *ApJ* 481, 500
 Ding M. D., Fang C., Huang Y. R., 1995, *Solar Phys.* 158, 81
 Ellison M. A., 1949, *MNRAS* 109, 3
 Emslie A. G., Mariska J. T., Montgomery M. M., Newton E. K., 1998, *ApJ* 498, 441
 Falchi A., Mauas P. J. D., 2002, *A&A* 387, 678
 Fisher G. H., 1989, *ApJ* 346, 1019
 Fisher G. H., Canfield R. C., McClymont A. N., 1985b, *ApJ* 289, 434
 Fisher G. H., Canfield R. C., McClymont A. N., 1985a, *ApJ* 289, 414
 Forbes T. G., Malherbe J. M., Priest E. R., 1989, *Solar Phys.* 120, 285
 Gan W. Q., Fang C., 1990, *ApJ* 358, 328
 Gan W. Q., Rieger E., Fang C., 1993, *ApJ* 416, 886

- Gan W. Q., Zhang H. Q., Fang C., 1991, *A&A* 241, 618
Heinzel P., 1995, *A&A* 299, 563
Heinzel P., Karlický M., Kotrč P., Švestka Z., 1994, *Solar Phys.* 152, 393
Ichimoto K., Kurokawa H., 1984, *Solar Phys.* 93, 105
Karlický M., Hénoux J.-C., 1992, *A&A* 264, 679
Kopp R. A., Pneuman G. W., 1976, *Solar Phys.* 50, 85
Machado M. E., Avrett E. H., Vernazza J. E., Noyes R. W., 1980, *ApJ* 242, 336
Mariska J. T., Emslie A. G., Li P., 1989, *ApJ* 341, 1067
Metcalf T. R., 1990, Ph.D. thesis, AA(California Univ., San Diego.)
Mihalas D., 1978, *Stellar atmospheres /2nd edition/,* San Francisco, W. H. Freeman and Co., 1978. 650
Nejezchleba T., 1998, *A&AS* 127, 607
Neupert W. M., 1968, *ApJ* 153, L59
Rybicki G. B., Hummer D. G., 1991, *A&A* 245, 171
Schmieder B., Forbes T. G., Malherbe J. M., Machado M. E., 1987, *ApJ* 317, 956
Tang F., 1983, *Solar Phys.* 83, 15
Švestka Z., Kopecký M., Blaha M., 1962, *Bulletin of the Astronomical Institutes of Czechoslovakia* 13, 37
Vernazza J. E., Avrett E. H., Loeser R., 1981, *ApJS* 45, 635
Wuelser J.-P., 1987, *Solar Phys.* 114, 115
Wuelser J.-P., Marti H., 1989, *ApJ* 341, 1088
Zarro D. M., Canfield R. C., 1989, *ApJ* 338, L33
Zarro D. M., Canfield R. C., Metcalf T. R., Strong K. T., 1988, *ApJ* 324, 582